Please cite this article in press as: Wu et al., Actin-Delimited Adhesion-Independent Clustering of E-Cadherin Forms the Nanoscale Building Blocks of Adherens Junctions, Developmental Cell (2015), http://dx.doi.org/10.1016/j.devcel.2014.12.003

Developmental Cell
Article

Actin-Delimited Adhesion-Independent Clustering of E-Cadherin Forms the Nanoscale Building Blocks of Adherens Junctions

Yao Wu,[1] Pakorn Kanchanawong,[1,2] and Ronen Zaidel-Bar[1,2,*]
[1]Mechanobiology Institute, National University of Singapore, Singapore 117411, Singapore
[2]Department of Biomedical Engineering, National University of Singapore, Singapore 117575, Singapore
*Correspondence: biezbr@nus.edu.sg
http://dx.doi.org/10.1016/j.devcel.2014.12.003

SUMMARY

E-cadherin is the major adhesion receptor in epithelial adherens junctions, which connect cells to form tissues and are essential for morphogenesis and homeostasis. The mechanism by which E-cadherin monomers cluster and become organized in adherens junctions remains poorly understood. Here, using superresolution microscopy techniques in combination with structure-informed functional mutations, we found that loosely organized clusters of approximately five E-cadherin molecules that form independently of *cis* or *trans* interactions, and that are delimited by the cortical F-actin meshwork, are the precursors of *trans*-ligated adhesive clusters that make up the adherens junction. The density of E-cadherin clusters was wide ranged, and notably, we could detect densities consistent with the crystal lattice structure at the core of adhesive clusters, which were dependent on extracellular domain interactions. Thus, our results elucidate the nanoscale architecture of adherens junctions, as well as the molecular mechanisms driving its assembly.

INTRODUCTION

A hallmark of the evolutionary transition from unicellular to multicellular animals was the appearance of classical cadherins, transmembrane adhesion receptors with cytoplasmic tails that can link to the actin cytoskeleton (Murray and Zaidel-Bar, 2014). Epithelial cadherin (E-cadherin) is the first classical cadherin to be expressed in the embryo, and it is essential for development as well as for maintaining epithelial integrity in the adult (van Roy and Berx, 2008), as evidenced by the fact that loss of E-cadherin is associated with several forms of cancer (Baranwal and Alahari, 2009; Carneiro et al., 2012).

E-cadherin fulfills its role as a mediator of cell-cell adhesion within distinct cellular structures termed "adherens junctions" (Harris and Tepass, 2010). In addition to physically connecting neighboring cells, adherens junctions function as signaling centers, responding to biochemical and mechanical stimuli from the environment by activating signaling pathways within the cadherin adhesome (McEwen et al., 2012; Zaidel-Bar, 2013). The formation of adherens junctions has been extensively studied using conventional light microscopy (Adams et al., 1998; Hong et al., 2010; Vasioukhin et al., 2000; Yamazaki et al., 2007). These studies have documented small puncta of E-cadherin that formed shortly after cells came into contact. These puncta later appeared to coalesce into a dense, mostly immobile plaque at the apical region of lateral membranes. It has been proposed that the lateral spot-like clusters of cadherin become incorporated into the apical belt-like adherens junction and that, following incorporation, they undergo a qualitative change in organization (Adams et al., 1996; Yonemura et al., 1995). However, the difference between spot-like lateral junctions and the apical junction has not been characterized quantitatively.

Within adherens junctions, E-cadherin receptors can engage via their extracellular domains with E-cadherin receptors on an opposing cell (*trans* interaction) as well as E-cadherin receptors from the same cell (*cis* interaction). The molecular nature of these interactions has been determined from crystal structures and structure-informed point mutations (reviewed in Brasch et al., 2012). The predominant *trans* interaction involves strand swapping, whereby a tryptophan residue from the first cadherin domain (EC1) of one protein becomes inserted into a hydrophobic pocket in the EC1 of the opposing cadherin and vice versa (Harrison et al., 2011; Shapiro et al., 1995). The *cis* interaction is mediated by an EC1-EC2 interface stabilized by a hydrophobic interaction between residues V81 and V175 (Harrison et al., 2011). Notably, the *cis* and *trans* interfaces are distinct, so a single cadherin can, in principle, simultaneously be engaged in one *trans* interaction and two *cis* interactions, forming strands on one cell that can interact with opposing strands to form a lattice (Harrison et al., 2011; Wu et al., 2011). Such lattices were observed in crystals of purified extracellular domains of E-cadherin, but whether such structures form between cells is an open question.

The initial formation of *trans* dimers between freely diffusing monomers was calculated to be a rare event, and in molecular dynamics simulations, the nucleation of a junction was only possible by invoking a "diffusion trap" (Zhang et al., 2009). How such a diffusion trap is achieved in cells is not known. Notably, single-molecule tracking of E-cadherin on the dorsal surface of cells with magnetic tweezers has produced evidence of constrained movement (Sako et al., 1998), leading to the hypothesis that E-cadherin receptors are corralled by actin cortex fences (Kusumi et al., 1999). The role that such actin fences

might play in the formation of adherens junctions has not yet been addressed. Here, we used superresolution microscopy techniques to study the nanoscale organization of E-cadherin, and we found that the basic subunit of E-cadherin adhesion is a cluster that forms independently of cadherin-cadherin interactions and is delimited by a "fence" of F-actin.

RESULTS

Lateral and Apical Adherens Junctions Are Both Composed of Nanosized Clusters of E-Cadherin

E-cadherin at the interface between polarized Eph4 mammary epithelial cells was immunolabeled and imaged by diffraction-limited confocal microscopy. We observed E-cadherin-positive structures of two forms: a condensed band along the apicalmost portions of lateral membranes and sparse puncta throughout the remainder of the lateral membranes (Figure 1A). The lateral puncta were most easily visualized in regions where neighboring cell membranes met at an oblique angle, as depicted schematically in Figure 1A'.

Next, we used single-molecule-based superresolution microscopy, fluorescence-photoactivated localization microscopy/stochastic optical reconstruction microscopy (F-PALM/STORM) (Betzig et al., 2006; Hess et al., 2006; Rust et al., 2006) to reconstruct nanoscale images of Eph4 cells immunolabeled for E-cadherin with a photoswitching fluorophore. A weak cylindrical lens in the light path introduced slight astigmatism, so that the Z position of each fluorophore could also be determined with subdiffraction accuracy (3D-STORM) (Huang et al., 2008). Using oblique illumination (Tokunaga et al., 2008), we gathered information on the organization of E-cadherin in both the apical and lateral E-cadherin structures at the depth of 0.3–1.0 μm.

The increase in resolution attained by 3D-STORM revealed that the apical junction, which appeared as a solid belt in conventional microscopy (Figure 1B), was actually made up of distinct clusters, tightly packed and evenly distributed along the cell-cell interface (Figure 1B'). It is interesting that E-cadherin below the apical junction ("lateral") formed clusters that qualitatively appeared very similar to the clusters observed in the apical junction, except that they were more sparsely distributed (Figures 1C and 1C').

The accuracy in the X-Y and Z coordinates in our superresolution images was assessed from the distribution of uncertainty of single-molecule localization (Thompson et al., 2002), and as shown in Figure 1D, the majority of fluorophores were localized with an X-Y accuracy of 30 nm or better and with a typical Z precision of ~106 nm.

The use of antibodies for labeling E-cadherin could potentially introduce quantification artifacts due to partial inaccessibility and variability in the dye-labeling ratio of secondary antibodies. To exclude the possibility of antibody-related artifacts, we imaged by 3D-STORM A431D cells (a line derived from A431 that lacks endogenous E-cadherin) stably expressing a recombinant E-cadherin fused with the photoswitchable protein Dendra2 (Hong et al., 2010). These cells show a configuration of E-cadherin similar to Eph4 cells, except that they were taller, and their lateral membranes, toward the bottom, were oriented in an almost flat angle relative to the coverslip (Figure S1A available online). 3D-STORM images of E-cadherin-Dendra2 in A431D cells showed essentially the same pattern of organization as immunolabeled E-cadherin in Eph4 cells (Figures S1B and S1C).

Quantitative Analysis of Apical and Lateral E-Cadherin Clusters Reveals a Wide Range of Densities

To quantitatively relate the number of E-cadherin molecules to the number of detected molecular events in Eph4 cells, the secondary antibodies conjugated to the photoswitchable fluorophore Alexa Fluor 647 were imaged after being separated by sonication and sparsely distributed on coverslips, and it was determined that 5.3 ± 0.25 detected single-molecule events correspond to each Alexa Fluor 647 fluorophore. Thus, single-molecule events corresponding to each individual antibody molecule can be identified.

To quantitatively analyze E-cadherin clusters and their nanoscale organization, we used the mean shift algorithm to group the E-cadherin signals in the superresolution data set into clusters. Mean shift clustering is a nonparametric iterative technique that does not require prior knowledge of the number of clusters and does not constrain their shape (Cheng, 1995; Comaniciu and Meer, 2002). Clusters identified by mean shift are local density maxima, and all points within an identified cluster converge to the same local maxima. Figure 2A depicts a representative 3D-STORM image of part of an apical junction in Eph4 cells, and Figure 2A' displays the output of the mean shift clustering for the same region.

Once clusters were defined, we determined the equivalent diameter of each cluster, the spacing between clusters, and the number of molecules per cluster in 1,281 clusters from ten junctions in three different cells. Histograms depicting the pooled data are shown in Figures 2B–2D. We found the median number of E-cadherin receptors per cluster to be six, the median cluster diameter to be 60 nm, and the median value for spacing between clusters to be 157 nm. A similar analysis performed for lateral clusters (Figures 2G–2J) confirmed that they have similar median equivalent diameter, but the median number of molecules per cluster (4.6) was slightly lower. As expected, the median spacing between clusters in lateral membranes (277 nm) was almost 1.75 times larger than in the apical junction.

The same analysis was performed on the 3D-STORM data collected using A431D cells expressing E-cadherin-Dendra2 (Figure S2). Most photoswitchable fluorophores, including photoactivatable fluorescent proteins (PA-FPs), exhibit complex multiple on-off "blinking" events that complicate direct quantification of molecule counts from the number of observed events (Annibale et al., 2011; Sengupta et al., 2011). Although Dendra2 appears somewhat less bright than other PA-FPs, previous photophysical characterization indicated that Dendra2 is comparatively suitable for molecule counting as it blinks less and bleaches faster (Lee et al., 2012). To calibrate the molecule count conversion ratio under our imaging conditions, we imaged very sparse E-cadherin-Dendra2 in membrane fragments, observing that 2.2 ± 0.082 detected single-molecule events correspond to each Dendra2 molecule in good agreement with previous measurements (Lee et al., 2012). Therefore, our approach enabled quantification of E-cadherin molecules observed in nanoscale clusters. The results obtained for lateral clusters were very similar to the Eph4 results, except that the cluster equivalent diameter was somewhat smaller (median, 52 nm; Figure S2B),

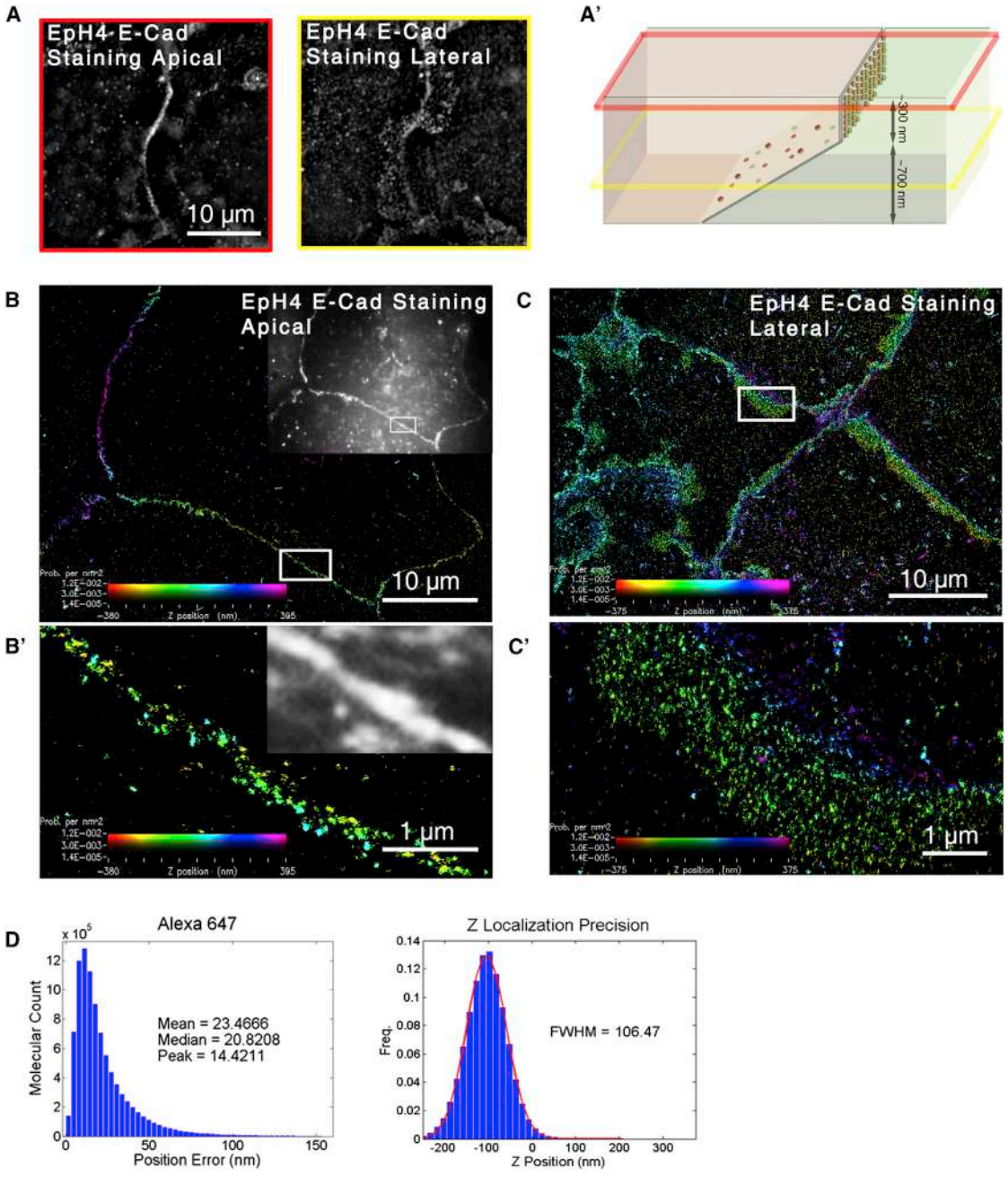

Figure 1. E-Cadherin in Both Apical and Lateral Adherens Junctions of Eph4 Cells Is Organized in Discrete Nanoscale Clusters

(A and A') In (A), conventional light microscopy views are shown of apical (red box) and lateral (yellow box) adherens junctions in Eph4 cells. (A') A schematic drawing of an entire cell-cell junction between Eph4 cells, illustrating with the red and yellow boxes at what position the images in (A) were taken. E-cad, E-cadherin.

(B and B') In (B), a 3D stochastic optical reconstruction microscopy (3D-STORM) image is shown of E-cadherin staining in an apical cell-cell junction (zonula adherens) between Eph4 cells (insert shows the diffraction limited image of the same cells). (B') An enlargement of the region marked in (B). In all 3D-STORM images, the Z position is color coded, and intensity indicates position accuracy according to the color bar in each panel.

(C and C') In (C), lateral junctions (puncta adherens) in Eph4 cells are stained for E-cadherin and imaged by 3D-STORM. (C') An enlargement of the region marked in (C).

(D) Quantification of the X-Y and Z position accuracies of the data points in all 3D-STORM images. Freq., frequency; FWHM, full width at half maximum.

likely because of the fact that E-cadherin was labeled by Dendra2 and not with primary and secondary antibodies that add their own dimensions to the apparent cluster area. The apical junction in A431D cells is substantially further away from the coverslip (~4.0 μm) compared to the apical junction in Eph4 cells, resulting in poorer resolution. This may account for the larger E-cadherin clusters obtained from the segmentation of the single-molecule events by the mean shift algorithm into

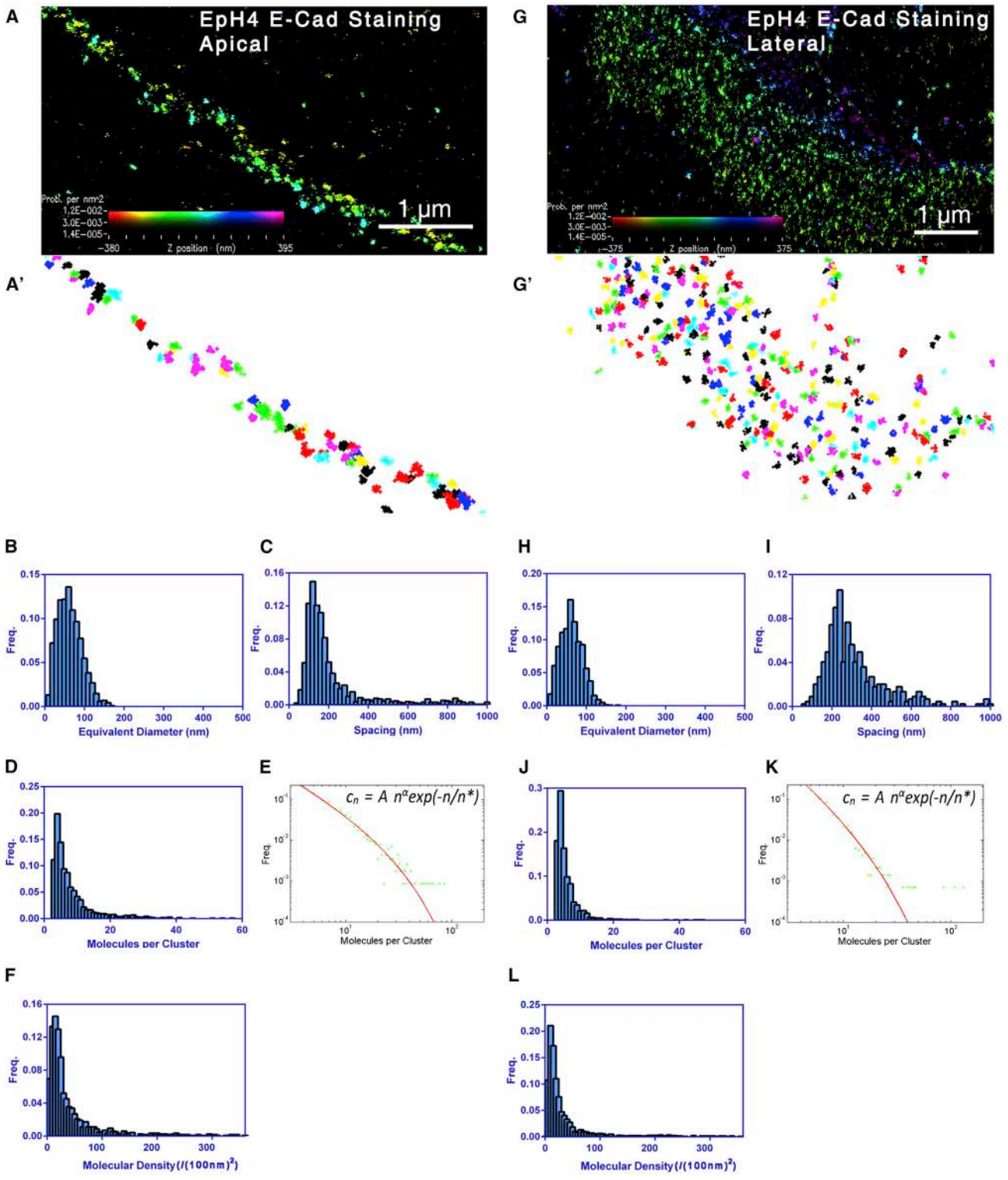

Figure 2. Quantification of Size, Spacing, Molecules per Cluster, and Density of Apical and Lateral E-Cadherin Clusters in Eph4 Cells Based on the Mean Shift Algorithm

(A and A') In (A), the same image is shown as in Figure 1B'. (A') The clusters map after analysis using the mean shift algorithm according to local density maxima. For visualization purposes, all points belonging to the same cluster were plotted with the same color. E-cad, E-cadherin.

(B–D) Frequency (Freq.) histograms for (B) the equivalent diameter of clusters, (C) the spacing between clusters, and (D) the number of E-cadherin molecules per apical cluster (n = 1,281 clusters from n = 10 junctions from n = 3 samples).

(legend continued on next page)

much larger E-cadherin clusters, with a median equivalent diameter of 112.97 nm (Figure S2H), although it may also reflect a true difference in organization between the two cell lines. Mean and median values of all quantitative parameters calculated for E-cadherin clusters in both cell lines are provided in Table S1.

A recent superresolution microscopy study of adherens junctions in *Drosophila* embryos observed that the distribution of cluster size, as measured by the number of E-cadherin molecules per cluster, followed a power law (Truong Quang et al., 2013). We examined the distribution of cluster size in both apical and lateral junctions of Eph4 and A431D cells and found that they could also be well approximated by a power law spanning two orders of magnitude (Figures 2E and 2K; Figures S2E and S2K). However, the distribution of cluster equivalent diameter did not follow a power law but rather was better approximated by a Gaussian distribution (Figures 2B and 2H; Figures S2B and S2H). Since the area of E-cadherin clusters did not scale in accordance with the number of molecules per cluster, this implied a spread in the range of cluster densities. Indeed, as shown in Figures 2F and 2L, the calculated densities of E-cadherin clusters ranged from 20 to 100 molecules/(100 nm)^2.

Subregions with Crystal Packing Densities Are Present within Adhesive E-Cadherin Clusters

The range of densities we calculated for E-cadherin clusters in both Eph4 and A431D cells was significantly lower than the density expected for a lattice of E-cadherin molecules arranged according to the crystal lattice (Harrison et al., 2011); ~360 molecules/(100 nm)^2. We hypothesized that some of the clusters classified by the mean shift algorithm might be heterogeneous, consisting of smaller subdomains, which may be composed of molecular oligomers packed at densities comparable to the crystal structure. To test this idea, we generated local density maps of apical junctions and lateral clusters of A431D cells expressing E-cadherin-Dendra2 using a range of bin sizes for the calculation of density around each molecule. A bin size of 60 × 60 nm^2 produced a density map in which clusters appeared very similar to the clusters generated by the mean shift algorithm at lateral junctions, and the highest density observed was 100 molecules/(100 nm)^2 (Figures 3A and 3B). However, by reducing the bin size to 30 × 30 nm^2, we were able to detect within some of the clusters a much denser central core, with up to 360 molecules/(100 nm)^2, corresponding to crystal-like packing density (Figures 3C and 3D).

To test whether the subregions displaying crystal packing densities correspond to clusters of E-cadherin interacting with each other via the *cis* and *trans* interfaces found in the crystal structure, we acquired 3D-STORM data for A431D cells expressing variants of E-cadherin-Dendra2 with point mutations that abrogate either the *cis* or *trans* interaction or strengthen the *trans* interaction (Harrison et al., 2011; Laur et al., 2002; Pertz et al., 1999). As expected, *cis*-abolishing V81D/V175D mutations resulted in the disappearance of subregions with crystal packing densities from the density map (Figure 3E). Similarly, the *trans*-abolishing W2A mutation also resulted in the loss of high-density subregions (Figure 3F). Conversely, strengthening the *trans* interaction with the D1A mutation led to a dramatic increase in the area of subregions displaying crystal packing densities (Figure 3G). Quantification of the median density values from multiple junctions confirmed a statistically significant difference between wild-type E-cadherin and the mutants (Figure 3H).

E-Cadherin Clusters Can Form Independently of Homophilic E-Cadherin Interactions

Although the clusters formed by *cis* and *trans* mutants of E-cadherin-Dendra2 did not contain subregions with densities corresponding to the crystal lattice organization, we were intrigued by the fact that they nonetheless did form lateral clusters with characteristics of area and size that were indistinguishable from wild-type E-cadherin-Dendra2 (Figures 4A and 4B; Figures S3A and S3B). This suggested that E-cadherin clusters formed independently of adhesive interactions with E-cadherin in adjoining cells. To test this possibility, we imaged full-length E-cadherin-Dendra2 on the free edges of A431D cells facing an open space in the monolayer and on the basal membrane of A431D cells spread on poly-L-lysine (Figure 4C; Figure S3D). Statistical analysis showed that the *cis* and *trans* mutants of E-cadherin, as well as E-cadherin at the free edge, formed clusters indistinguishable from those formed by wild-type E-cadherin at lateral cell-cell junctions in terms of size and spacing and only slightly less dense (Figure 4D; Figures S3C–S3E). We verified that the observed clusters are at the plasma membrane and not in vesicles within the cell by immunolabeling nonpermeabilized cells with an antibody against the extracellular domain of E-cadherin and observing the same clusters as with the Dendra2 tagged E-cadherin (data not shown).

The observation that E-cadherin clusters formed independently of *trans*-ligation suggested that clustering depends on interactions of the cytoplasmic tail. However, the extracellular domain could potentially engage in interactions other than the *cis* and *trans* interactions identified in crystal structures. To rule out this possibility, we engineered and expressed in A431D cells a headless mutant of E-cadherin, which is missing all five extracellular cadherin domains. Headless E-cadherin localized throughout the plasma membrane, and, as expected, it did not facilitate the formation of any cell-cell junctions in A431D cells (Figure S3F). Remarkably, the headless mutant formed clusters at the membrane that were only smaller than the clusters found in the *cis* and *trans* mutants or with full-length E-cadherin along the cell free edge, confirming that the initial clustering of E-cadherin is dependent on cytosolic factors and independent of the extracellular domain.

(E) Log-log plot of the frequency of number of E-cadherin molecules per apical cluster fitted by a power law curve.
(F) Frequency histogram of the molecular densities of apical clusters.
(G and G') In (G), the same image is shown as in Figure 1C'. (G') The clusters map after analysis using mean shift algorithm according to local density maxima.
(H–J) Frequency histograms for (H) the equivalent diameter of clusters, (I) the spacing between clusters, and (J) the number of E-cadherin molecules per lateral cluster (n = 1,513 clusters from n = 12 junctions from n = 4 samples).
(K) Log-log plot of the frequency of number of E-cadherin molecules per cluster fitted by a power law curve.
(L) Frequency histogram for the molecular densities of lateral clusters.

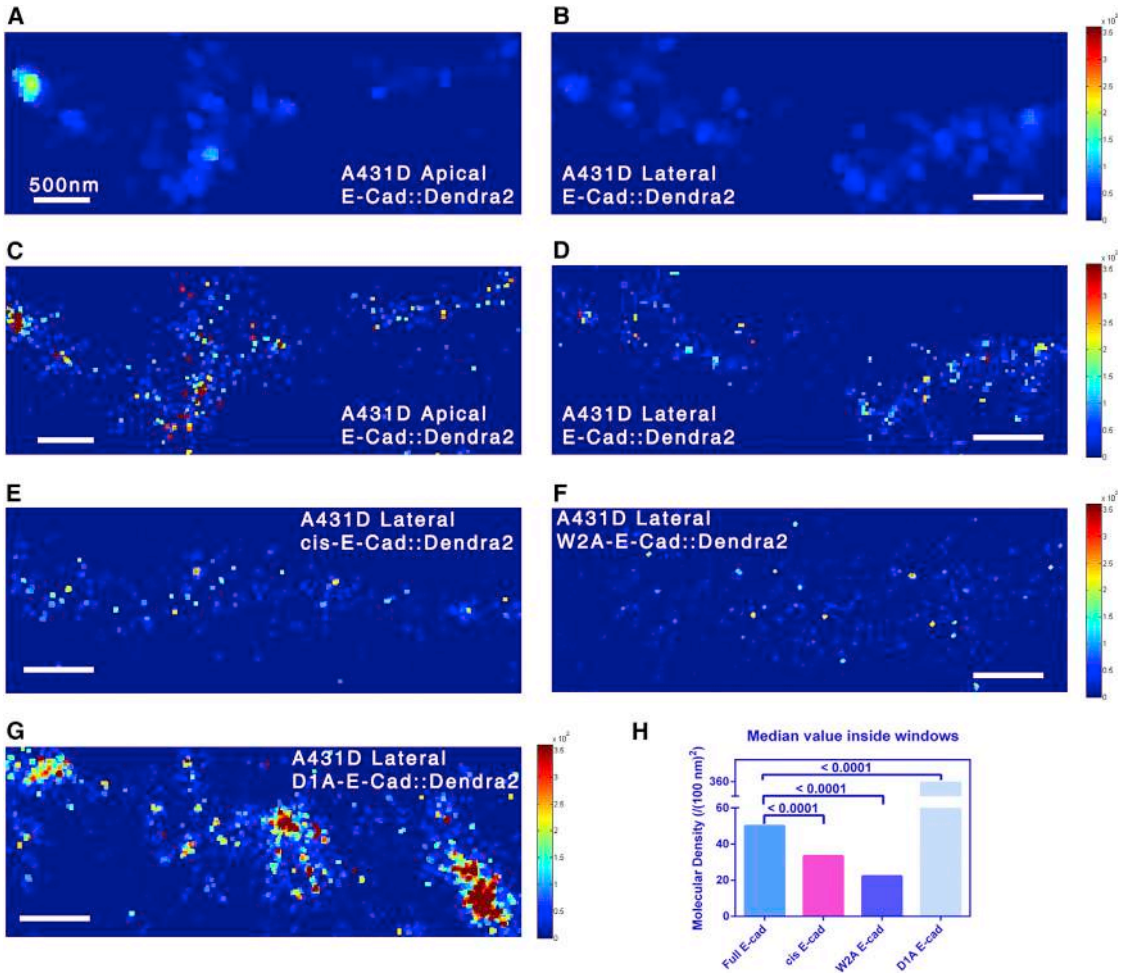

Figure 3. Density Maps of Adherens Junctions in A431D Cells Expressing Full-Length E-Cadherin-Dendra2 and Mutants in *cis* and *trans* Interactions Reveal Subregions with Crystal Packing Densities

(A) Apical junction density map of E-cadherin-Dendra2 in A431D cells, calculated using a bin size of 60 × 60 nm^2. E-cad, E-cadherin.

(B) Lateral junction density map of E-cadherin-Dendra2 in A431D cells, calculated using a bin size of 60 × 60 nm^2

(C) Apical junction density map of E-cadherin-Dendra2 in A431D cells, calculated using a bin size of 30 × 30 nm^2 and exhibiting subregions with densities comparable to crystal packing density.

(D) Lateral junction density map of E-cadherin-Dendra2 in A431D cells, calculated using a bin size of 30 × 30 nm^2.

(E and F) Lateral junction density maps of E-cadherin-Dendra2 with *cis*-abolishing V81D/V175D mutations in (E) EC1 and EC2 domains or (F) the *trans*-abolishing W2A mutation in the EC1 domain, calculated using a bin size of 30 × 30 nm^2 and showing no subregions of comparable densities to crystal packing density.

(G) Lateral junction density map of E-cadherin-Dendra2 with the *trans*-enhancing D1A mutation, calculated using a bin size of 30 × 30 nm^2 showing larger subregions with crystal packing densities. Density is color coded according to the color bar on the right.

(H) Comparison of the median value inside 30 × 30 nm^2 bins calculated from five density maps for each cell line. A nonparametric Mann-Whitney test was used to compare the median density values for full-length E-cadherin-Dendra2, its *cis* mutant, W2A mutant, and D1A mutant.

Considering that, based on their morphology, nonadhesive clusters can appear indistinguishable from adhesive clusters, we sought out a method to determine which E-cadherin clusters observed at cell-cell junctions are truly engaged in adhesive interactions with clusters in opposing cells and which clusters are nonadhesive. To this end, we performed a coculture experiment using A431 and A431D cells, which allowed us to uniquely label E-cadherin in each cell line and determine whether a cluster in one cell is matched by a cluster in the neighboring cell or not. We utilized the fact that recombinant E-cadherin-Dendra2 contains a small internal deletion (AA772–AA792), which eliminates the epitope for the anti-E-cadherin antibody C20820 (Hong et al., 2010). Thus, when A431 cells were cocultured with A431D cells expressing E-cadherin-Dendra2, the anti-E-cadherin antibody labeled only E-cadherin in the A431 cells, while Dendra2 reported uniquely on E-cadherin in the A431D cells. Junctions between the two cell types were imaged using 3D-STORM, and representative images for apical and lateral clusters are shown in Figures 4E and 4F. As expected, in the apical junction, the majority of clusters in A431D cells were closely matched by clusters in the neighboring A431 cell, suggesting that they are adhesive clusters (Figure 4E). In contrast, at the lateral interface, most of the clusters in one cell were not matched by a cluster in the neighboring cell, indicating

that they were nonadhesive (Figure 4F). In order to quantify the number of presumed adhesive and nonadhesive clusters, we performed mean shift analysis for each label separately. In apical junctions, which were close to an angle of 90° relative to the imaging plane, we considered neighboring clusters within 100 nm (the length of two extended E-cadherin molecules) to be adhesive. In lateral junctions, which were slanted at an angle of 15° relative to the imaging plane, we considered clusters that appear to overlap or be in contact with a cluster in the other cell as putative adhesive and those that were separated from all clusters in the other cell as nonadhesive. The result of such quantification of 2,682 clusters in 19 junctions revealed that 74.8% of clusters in the apical junction are putatively adhesive, whereas only 19.4% of the lateral clusters were identified as putative adhesive clusters. We found that, in the lateral junction regions, the size distributions of adhesive and nonadhesive clusters were similar to each other, whereas the average molecular density of adhesive clusters was about three times higher than nonadhesive clusters (Figures 4F''–4H).

E-Cadherin Clusters Are Delimited by F-Actin

Our finding that E-cadherin clusters formed independently of extracellular interactions raised the question on the mechanism responsible for the confinement of E-cadherin within clusters. Previous work suggested that E-cadherin mobility at the membrane may be confined by "fences" of cortical F-actin (Kusumi et al., 1999; Sako et al., 1998), with a mesh size of 50–200 nm (Morone et al., 2006). Hence, we investigated the relationship between F-actin and E-cadherin organization at the plasma membrane by costaining A431D cells expressing full-length E-cadherin-Dendra2 with a high concentration of phalloidin-Alexa Fluor 647. We imaged a region of the cell-cell interface that is nearly parallel to the observation plane so that the relative position of E-cadherin and F-actin could be determined most accurately. As shown in Figures 5A and 5B, the 3D-STORM imaging clearly showed that, at the nanoscale resolution, F-actin and E-cadherin were predominantly mutually exclusive. Based on their Z positions, we determined that the E-cadherin cytoplasmic tails and F-actin were positioned at the same plane (Figure 5C). We quantified the degree of colocalization between F-actin and E-cadherin in our images and found it to be 0.076 (Mander's coefficient). Figure 5D contains several examples of the relationship between E-cadherin and F-actin at lateral regions of the membrane. The predominant phenomenon observed is that of an F-actin meshwork surrounding E-cadherin clusters. A potential caveat with these images is that the F-actin we observed is contributed by both cells making up the junction. To overcome this issue, we coimaged F-actin and E-cadherin clusters at junction-free edges of A431D cells expressing full-length E-cadherin-Dendra2, and we found the same organization, namely, an F-actin meshwork surrounding E-cadherin clusters (Figures 5E–5G).

We also examined the relationship between F-actin and E-cadherin in apical junctions. There, in addition to the F-actin meshwork surrounding E-cadherin clusters, we identified F-actin bundles further away from the membrane. The relative positions of E-cadherin and F-actin in the images of the apical junction are shifted compared to lateral clusters because the observation angle relative to the membrane is shifted by almost 90°, but they remained, for the most part, mutually exclusive (Figures 5H–5J).

The observation of an F-actin meshwork surrounding E-cadherin clusters was consistent with the hypothesis that F-actin functions as a corral (Kusumi et al., 1999; Sako et al., 1998). To test this hypothesis directly, we used two complementary approaches. First, we used an actin monomer-sequestering compound latrunculin A to disrupt the cortical F-actin meshworks in A431D cells expressing full-length E-cadherin-Dendra2; second, we examined A431D cells expressing a mutant of E-cadherin-Dendra2 that is lacking the cytoplasmic tail.

As shown in Figure 6A, latrunculin A treatment resulted in a substantial increase in the size and area of E-cadherin clusters. We quantified 213 clusters from three cells and found a 1.8-fold increase in the median number of E-cadherin molecules per cluster and a 5-fold increase in their median area, resulting in a 3-fold decrease in density compared to cells with an intact F-actin cytoskeleton (Figure 6C; Figure S4A). We observed an even larger expansion of cluster size and area with the tailless mutant of E-cadherin (Figures 6B, 6C, and S4B). Notably, labeling of the cells treated with latrunculin A with phalloidin confirmed that the majority of the F-actin meshwork was gone, while thick actin bundles appeared to coalesce at cell-cell junctions, and, also notably, the large E-cadherin clusters colocalized with the F-actin bundles (Figures 6D–6F). Furthermore, dual-label imaging of the tailless mutant with F-actin revealed that, in this case, the two labels no longer exclude each other (Figures 6G–6I). Quantification of the degree of colocalization of tailless E-cadherin with F-actin gave a value of 0.497 (Mander's coefficient).

Homophilic Interactions of the Extracellular Domain Also Play a Role in E-Cadherin Clustering

Our results showed that full-length E-cadherin can form clusters independently of *cis* or *trans* interactions of the extracellular domain (Figures 4A–4D), which suggests a clustering mechanism that depends on the cytoplasmic tail. However, tailless E-cadherin mutants also form clusters (Figure 6C). We hypothesized that *cis* and *trans* interactions of the extracellular domains, although not essential for clustering in the context of full-length E-cadherin, were the driving force clustering tailless E-cadherin. If that were the case, we would expect E-cadherin in the tailless clusters to form oligomers at crystal lattice density. We generated density maps (bin size, 30 nm) of tailless E-cadherin in A431D cells, and, as expected, we found within the large clusters identified by the mean shift algorithm vast swaths of E-cadherin packed at densities compatible with the crystal lattice (Figure 7A). We further tested the role of homophilic interactions in the tailless E-cadherin by acquiring 3D-STORM data of cell-cell junctions in A431D cells expressing tailless E-cadherin-Dendra2 constructs with point mutations in their extracellular domains abolishing either *cis* or *trans* interactions (Harrison et al., 2005, 2011; Troyanovsky et al., 2003). As shown in Figures 7B and 7C, both *cis* and *trans* mutations led tailless E-cadherin to exhibit a homogeneous distribution lacking any sign of clustering, confirming that homophilic interactions of the extracellular domain play a role in E-cadherin clustering, in parallel with a clustering mechanism that is cytoplasmic tail dependent. Finally, these results also serve as a control for all our experiments with

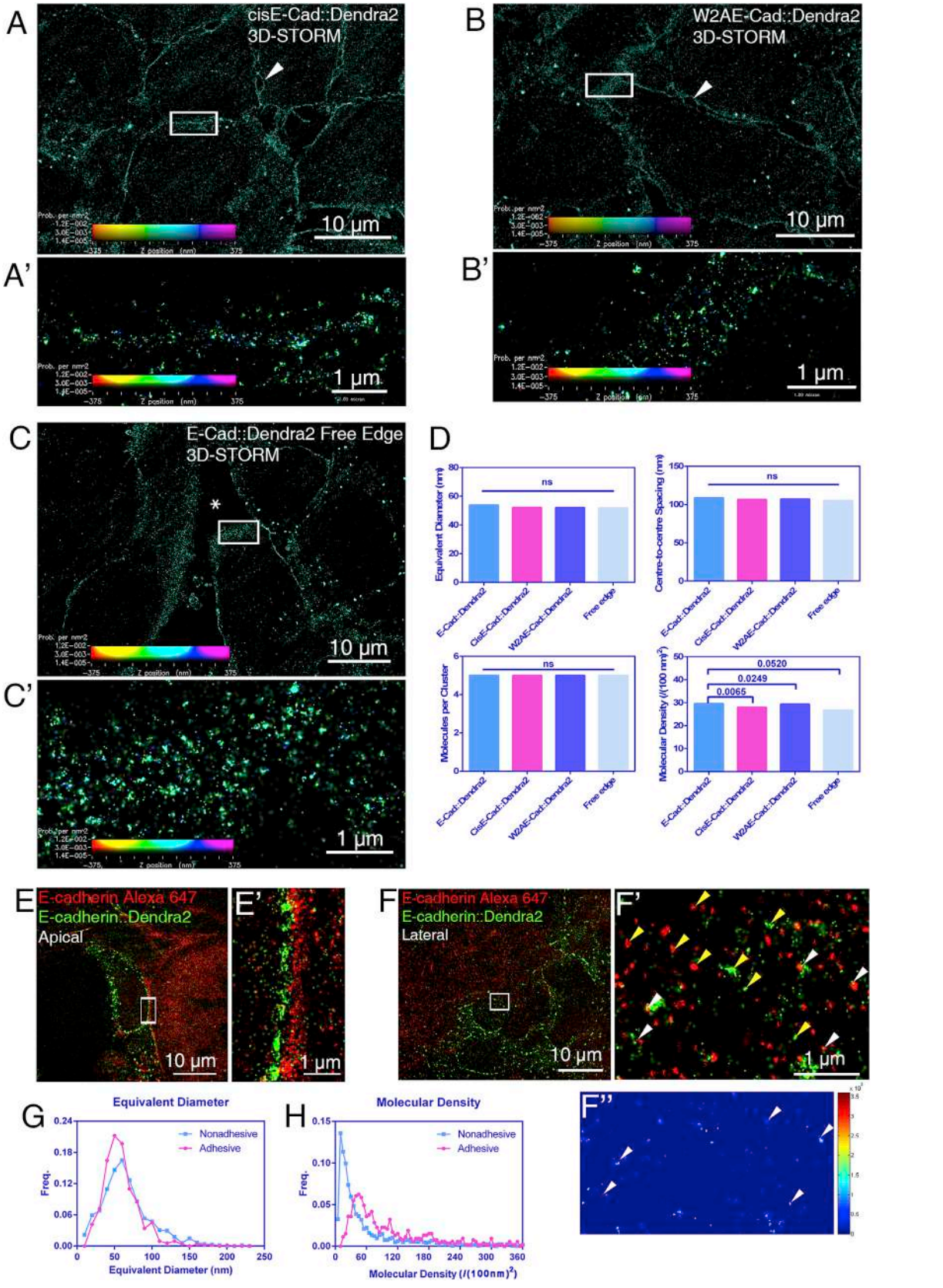

(legend on next page)

Dendra2-tagged E-cadherin. Although oligomerization of PA-FP tags may potentially lead to clustering, the lack of clustering in the *cis* and *trans* tailless mutants suggest that any contribution from Dendra2 oligomerization in our system is likely negligible.

DISCUSSION

E-cadherin clusters have been described during the initial stages of cell-cell contact (Adams et al., 1996, 1998; Vasioukhin et al., 2000) and in the lateral region of cell-cell junctions (Hong et al., 2010; Yonemura et al., 1995). The clusters observed in these studies, using diffraction-limited light microscopy, had a diameter of 0.3–0.7 μm. The mean equivalent diameter of the E-cadherin clusters we describe here was 52–60 nm, which is 10-fold smaller. However, since the resolution of our approach is ~10-fold better than conventional diffraction-limited microscopy, it is likely that we are describing the same structures. Noteworthy, the clusters we observed have the same dimensions as the minimal structural unit observed by electron microscopy in early cell-cell junctions (Miyaguchi, 2000; Yonemura et al., 1995).

Both light and electron microscopy studies have shown that, over time, E-cadherin clusters come closer together to form larger adhesion surfaces. It has been speculated that the formation of a mature adherens junction is accompanied by a qualitative change in cadherin organization from clusters to a uniform distribution. Our data do not support this hypothesis since, with our improved resolution, we continued to distinguish distinct E-cadherin clusters even in mature apical junctions, and those clusters had the same size distribution as lateral clusters. Thus, even as E-cadherin clusters became more densely packed, they remained separate entities. Our observation that each E-cadherin cluster is surrounded by F-actin led us to speculate that the F-actin meshwork may act as an insulator to prevent clusters from fusing with each other, but this remains a hypothesis that needs to be tested further. What process drives the packing of E-cadherin clusters within the apical junction? The static nature of 3D-STORM imaging did not allow us to address this question, but previously, the Takeichi and Troyanovsky groups had shown an active movement of cadherin clusters along F-actin cables in a basal-to-apical direction in A431D cells expressing VE- or E-cadherin (Hong et al., 2010; Kametani and Takeichi, 2007). Assuming the existence of a mechanism to stabilize cadherin clusters once they arrive at the apical junction, such as binding to F-actin cables (Cavey et al., 2008), such cadherin flow could explain the closer packing of cadherin clusters at the apical junction.

An important question in the field of cell-cell adhesion is: what is the basic subunit of adhesion? Based on single-molecule imaging of E-cadherin-GFP, Iino et al. proposed that E-cadherin oligomerizes independently of cell-cell adhesion and that these oligomers are the basic building blocks of adherens junctions (Iino et al., 2001). This notion did not garner further support, and the field, influenced by the crystal structures of E-cadherin and in vitro single-molecule experiments (Harrison et al., 2011; Pertz et al., 1999; Shapiro et al., 1995; Troyanovsky, 2005; Zhang et al., 2009), has adopted the view that the basic subunit of adhesion is an E-cadherin monomer. According to this view, in the absence of cell-cell contact, E-cadherin receptors are distributed over the plasma membrane in monomeric form. Contact with another E-cadherin-presenting cell facilitates the formation first of homophilic *trans* dimers, and only then the *trans* dimers interact in *cis* to form clusters (Brasch et al., 2012). Our superresolution mapping of E-cadherin at the plasma membrane and within adherens junctions provides strong supports for a model in which the basic unit of adhesion is a loose cluster of E-cadherin that forms independently of cell-cell contact.

The idea that E-cadherin within adherens junctions interacts with other E-cadherin molecules in the same way as it was found to interact in the crystal structure gained support from experiments in which the residues that mediate *cis* or *trans* interactions were mutated in tailless E-cadherin and cell-cell junctions were lost (Harrison et al., 2011). However, as others have noted before (Harris and Tepass, 2010; Troyanovsky, 2012), the overall density of E-cadherin molecules at adherens junctions, based on light and electron microscope imaging, was estimated to be in the range of 14–24 molecules/(100 nm)^2 (Hirokawa and Heuser, 1981; McGill et al., 2009; Miyaguchi, 2000), which is ~15-fold smaller than the density of 360 molecules/(100 nm)^2 predicted by the crystal structure (Harrison et al., 2011) (including E-cadherin from both sides of the junction). We believe that our data solve this conundrum. Using superresolution microscopy to individually localize all E-cadherin receptors within an adherens

Figure 4. E-Cadherin Clusters Form Independently of *cis* and *trans* Interactions of the Extracellular Domain

(A and A') In (A), 3D-STORM was used to image A431D cells expressing full-length E-cadherin-Dendra2 with the *cis*-abolishing V81D/V175D mutations in its EC1 and EC2 domains. The white arrow indicates opening of junctions, showing weakened junctions in this cell line. (A') A higher magnification of the region marked in (A). E-cad, E-cadherin.

(B and B') In (B), a 3D-STORM image shows A431D cells expressing full-length E-cadherin-Dendra2 with the *trans*-abolishing W2A mutation in its EC1 domain. The white arrow indicates opening of junctions, showing weakened junctions in this cell line. (B') A higher magnification of the region marked in (B).

(C and C') In (C), a 3D-STORM image shows cell edges from A431D cells expressing full-length E-cadherin-Dendra2. (C') A higher magnification of the region marked in (C). An asterisk marks the opening in the monolayer.

(D) Statistical analysis of cluster diameter, spacing between neighboring clusters, molecules per cluster, and molecular densities among full-length E-cadherin, different mutants, and cell edges. The bar charts show median values.

(E and E') In (E), a 3D-STORM image shows an apical junction between an A431 cell and an A431D cell expressing E-cadherin-Dendra2. The E-cadherin antibody staining (Alexa Fluor 647) recognizes E-cadherin in A431 cells only. (E') An enlargement of the region marked in (E).

(F–F'') In (F), a lateral junction is shown between A431 and A431D cells imaged by 3D-STORM using the same method as in (E). (F') An enlargement of the region marked in (F). (F'') The density map for the region in (F'). Yellow arrows in (F') point to nonadhesive clusters, and white arrows in (F') and (F'') point to adhesive clusters.

(G and H) Frequency distributions for (G) the equivalent diameter and (H) the molecular density for adhesive and nonadhesive lateral clusters, identified by the mean shift analysis (n = 2,528 clusters from n = 15 junctions from n = 5 samples).

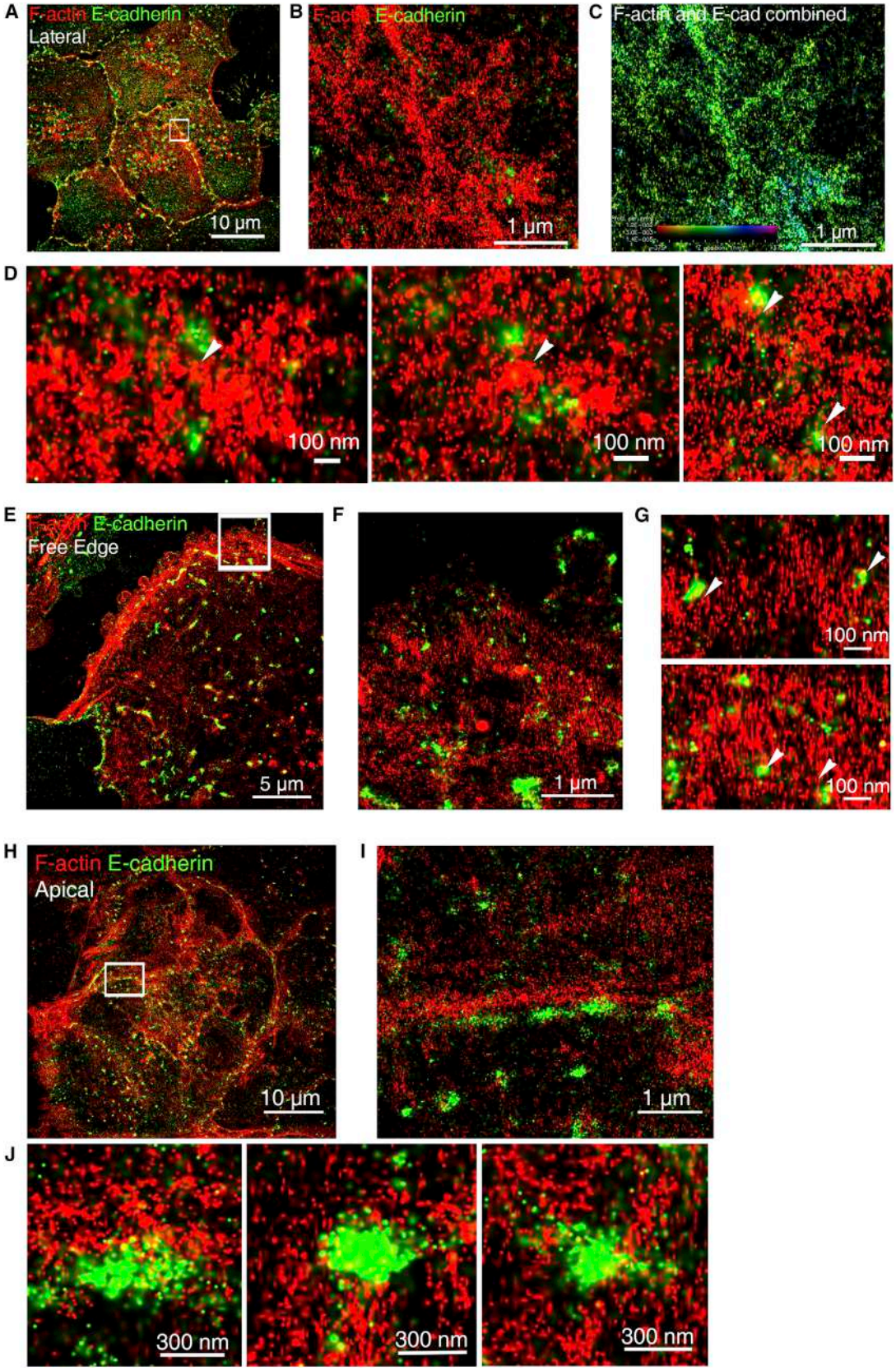

(legend on next page)

junction, we were able to confirm the existence of E-cadherin packed at crystal lattice densities, but notably, such high densities were observed only in small regions of the junction (100–900 nm^2) that existed as subregions within larger E-cadherin clusters. The median density of these larger clusters was 29.6 molecules/$(100\ nm)^2$, which is similar to the upper value obtained by previous methods (Hirokawa and Heuser, 1981; McGill et al., 2009; Miyaguchi, 2000).

Based on their overall density it is clear that the E-cadherin clusters we identified here are not made up entirely of crystal lattice packed molecules, which raises the questions: What drives their formation, and how are their borders defined? The results of our experiments with E-cadherin mutants suggest that clustering can be driven by either the extracellular domain or the cytosplasmic tail, and in wild-type E-cadherin it is probably driven by both. Thus, abolishing either *cis* or *trans* interactions by point mutations in the extracellular domain or deletion of the entire extracellular domain did not inhibit the formation of E-cadherin clusters. This result is consistent with our finding that the majority of lateral E-cadherin clusters are nonadhesive. In these cases, we presume that clustering is driven by the cytoplasmic tail. Although a molecular mechanism for tail-driven clustering has not yet been described, it has been reported previously for C- and N-cadherin (Katz et al., 1998; Yap et al., 1998) and, presumably, involves one or more of the adaptor proteins interacting with the E-cadherin tail (Petrova et al., 2012) and/or its indirect interaction with F-actin (Cavey et al., 2008). Nevertheless, deletion of the cytoplasmic tail does not prevent clustering. Previous work suggested that clustering of the tailless E-cadherin is driven by homophilic interactions of the extracellular domain (Harrison et al., 2011). Our findings support this idea, as the density of tailless E-cadherin clusters is consistent with crystal lattice density. Furthermore, *cis* and *trans* mutations in a tailless E-cadherin resulted in its complete inability to form clusters. It is noteworthy that mutations in either a *cis* or a *trans* interaction gave essentially the same result, in line with the idea that the two interactions act cooperatively in the process of E-cadherin clustering, as has been proposed by modeling (Wu et al., 2011).

Notably, tail-deleted E-cadherin formed substantially larger clusters than the full-length protein, indicating that, in addition to driving clustering, the tail also plays a restraining role with regard to cluster size. Moreover, we found that this restriction is, at least in part, due to the presence of an F-actin cortical meshwork, as depolymerization of the F-actin cortex resulted in similar expansion of E-cadherin clusters. It has long been known that F-actin plays an important role in organizing and stabilizing E-cadherin clusters (Adams et al., 1996; Cavey et al., 2008; Chu et al., 2004; Hong et al., 2013; Kovacs et al., 2002; Vasioukhin et al., 2000). It has been proposed that F-actin templates E-cadherin clusters by providing binding sites along the filaments. However, our dual-color 3D-STORM imaging of F-actin and E-cadherin revealed a very different relationship. We found full-length E-cadherin clusters to be surrounded by F-actin, with very little overlap between the two proteins, whereas the tailless E-cadherin mutant was equally likely to overlap with the F-actin meshwork. Thus, it appears that the cortical F-actin meshwork serves as a mold for E-cadherin clusters to form within its spaces. The notion of the F-actin cortex acting as a corral for E-cadherin clusters was previously suggested by Kusumi and colleagues based on single-molecule tracking and optical tweezers (Kusumi et al., 1999; Sako et al., 1998). We hypothesize that partitioning of E-cadherin into preadhesion clusters may be an ultrastructural prerequisite of E-cadherin ligation and represents the ''diffusion trap'' predicted by Honig and colleagues (Zhang et al., 2009). It is important to note that the mutual exclusion between E-cadherin and cortical F-actin we described does not contradict the notion of E-cadherin interacting with noncortical F-actin (Ratheesh and Yap, 2012). Indeed, we identified additional bundles of F-actin at apical adherens junctions, and their relationship with E-cadherin clusters will be the subject of future investigations.

In conclusion, our superresolution data support a model in which E-cadherin organizes into distinct nanoscale precursor clusters that mature into adhesive contacts. Preorganization into loosely packed nanoscale clusters appears to be independent of cell-cell contact and predominates in lateral junctions. The effects of the cytoplasmic tail deletion and actin disruption suggest that these clusters may arise through extracellular domain association and are delimited by the cortical F-actin meshwork, which partition the plasma membranes into corrals on the scale of 100–200 nm. Adhesive interactions between neighboring cells promote the compaction of the precursor clusters into adhesive clusters via *cis* and *trans* interactions, resulting in dense oligomeric cores with crystal packing density and that are highly enriched at adherens junctions. The nature of the interactions between E-cadherin and cytoplasmic adaptors that actuate this compacting transition, and whether this process is influenced by mechanical tension, remains an open question and a subject of further studies. Our results suggest that the cortical F-actin geometry and, perhaps, membrane domain organization specify the size scale of the loose precursor clusters, while the oligomeric scale of the dense adhesive core may be limited by steric interactions between the cytoplasmic partners of E-cadherin. The hierarchical and modular organization of

Figure 5. E-Cadherin Clusters Are Surrounded by F-Actin

(A) A431D cells expressing E-cadherin-Dendra2 costained for F-actin with phalloidin-Alexa Fluor 647 and imaged by 3D-STORM at lateral membrane.

(B) Enlarged 3D-STORM image of the cell-cell junction region demarcated in (A) showing mutual exclusive localization of E-cadherin (green) and F-actin (red).

(C) Molecular coordinates from both F-actin and E-cadherin (E-cad) channels were plotted together and color coded according to their Z position in order to distinguish their relative localization in terms of height.

(D) Examples of individual E-cadherin clusters and associated F-actin at lateral membranes.

(E) A431D cells expressing E-cadherin-Dendra2 (green) costained for F-actin (red) with phalloidin-Alexa Fluor 647 and imaged by 3D-STORM at cell edges.

(F) An enlargement of the region marked in (E).

(G) Examples of individual E-cadherin clusters and associated F-actin at cell edges.

(H) A431D cells expressing E-cadherin-Dendra2 costained for F-actin with phalloidin-Alexa Fluor 647 and imaged by 3D-STORM at apical junctions.

(I) An enlargement of the region marked in (H).

(J) Examples of individual E-cadherin clusters and associated F-actin at apical junctions.

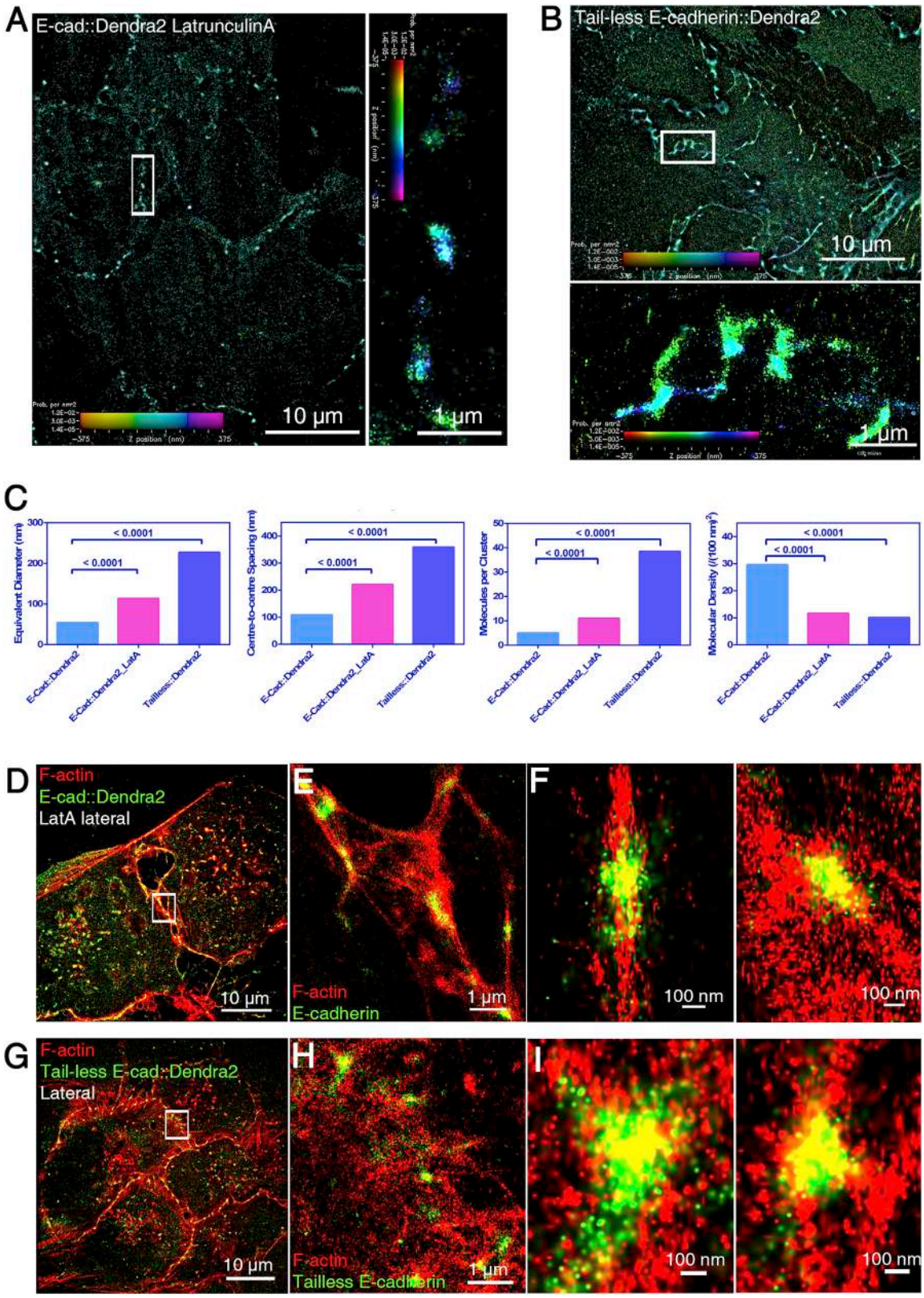

Figure 6. F-Actin Depolymerization or Deletion of the Cytoplasmic Tail Result in the Growth of E-Cadherin Clusters

(A) 3D-STORM image of A431D cells expressing full-length E-cadherin-Dendra2 treated with latrunculin A (0.2 μg/ml) for 20 min, exhibiting larger than normal clusters. E-cad, E-cadherin.

(legend continued on next page)

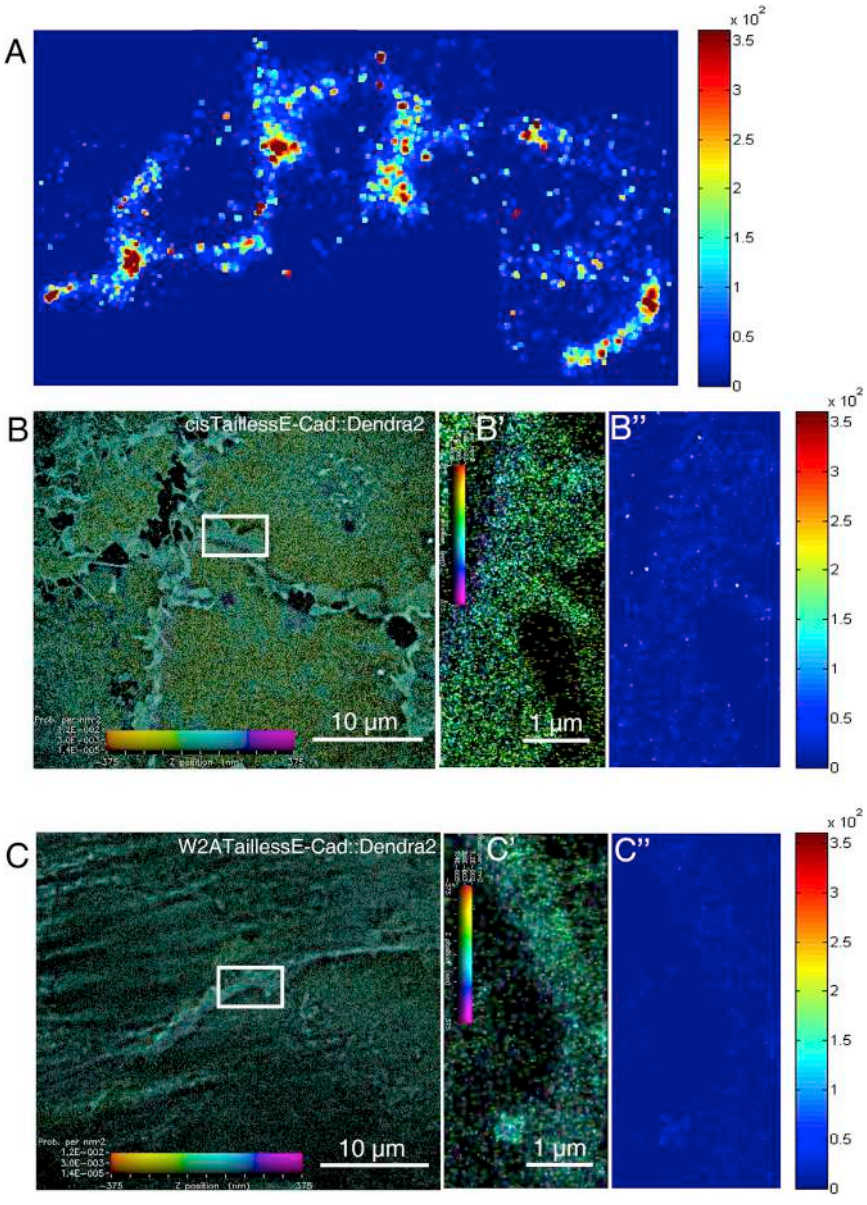

Figure 7. Tailless E-Cadherin with *cis*- or *trans*-Abolishing Mutations Cannot Form Clusters

(A) Density map of lateral junction of tailless E-cadherin-Dendra2 calculated using a bin size of 30 × 30 nm^2. Density is color coded according to the color bar on the right.

(B–B'') In (B), a 3D-STORM image is shown of A431D cells expressing the tailless E-cadherin-Dendra2 with the *cis*-abolishing V81D/V175D mutations in its EC1 and EC2 domains. (B') An enlargement of the region in (B). (B'') A density map of the same region in (B'). E-cad, E-cadherin.

(C–C'') In (C), a 3D-STORM image shows A431D cells expressing the tailless E-cadherin-Dendra2 with the *trans*-abolishing W2A mutation in its EC1 domain. (C') An enlargement of the region marked in (C). (C'') A density map of the same region in (C').

E-cadherin could contribute to the adaptive plasticity of adherens junctions, which are frequently called for in a living animal.

EXPERIMENTAL PROCEDURES

Information on cell culture, plasmids, immunohistochemistry, latrunculin A treatment, and characterization of photoswitching properties is available in the Supplemental Experimental Procedures.

Sample Preparation for Superresolution Imaging

Cells were cultured either on sterile #1.5 coverslips containing sparsely adsorbed plasmonic gold nanoparticle fiducials immobilized by ~50 nm of sputtered SiO_2 (Hestzig) or on precleaned #1.5 coverslips without pre-embedded fiducial markers. For the latter, 80–100 nm gold nanoparticles (Corpuscular, 790122-010) were incubated with the samples prior to imaging to serve as fiducial marks. Fixed cells were mounted in a PBS-based imaging buffer containing oxygen scavenger, made fresh before imaging: 45 mM Tris-HCl, 9.4 mM NaCl, 9% glucose, 100 mM mercaptoethylamine, 0.56 mg/ml glucose oxidase, and 0.034 mg/ml catalase. The imaging samples were assembled by placing a clean coverslip on top of the cell-containing coverslip. Excess imaging buffer was then removed, and the samples were sealed by nail polish.

Acquisition and Processing of Superresolution Data Sets

Single-molecule image acquisition was performed on a Nikon N-STORM microscope equipped with a piezo z stage (Mad City Labs), an iXon3 512 × 512 pixel EMCCD camera (Andor), a cylindrical lens insert for astigmatism-based 3D imaging, 561 nm/150 mW laser for Dendra2, 640 nm/100 mW laser for Alexa Fluor 647, and 405 nm/50mW for photoactivation. The objective lens used was Nikon 100× Apo total internal reflection fluorescence, NA 1.49. A total of 30,000 frames were acquired for each data set. For Alexa Fluor 647 imaging, raw images were acquired using continuous laser illumination (640 nm) at 30 frames per second. For Dendra2 imaging, the sample was continually illuminated with 561 nm laser in conjunction with pulsed illumination of the 405 nm laser for photoconverting Dendra2 from green emitting to red emitting, at 30 frames per seconds. To reduce out-of-focus

(B) 3D-STORM image of A431D cells expressing an E-cadherin-Dendra2 deletion mutant missing its cytoplasmic tail ("tailless") forming large clusters.
(C) Statistical analysis of cluster diameter, spacing between neighboring clusters, molecules per cluster, and molecular densities among full-length E-cadherin, latrunculin A treatment, and tailless E-cadherin. The bar charts show median values.
(D) Dual-color 3D-STORM image of latrunculin-A (LatA)-treated A431D cells expressing full-length E-cadherin-Dendra2 (green) with phalloidin staining (red).
(E) An enlargement of the region marked in (D).
(F) Further enlargements of individual E-cadherin clusters and F-actin.
(G) Dual-color 3D-STORM image of A431D cells expressing a tailless E-cadherin-Dendra2 with phalloidin staining.
(H) An enlargement of the region marked in (G).
(I) Further enlargements of individual tailless E-cadherin clusters and F-actin.

background fluorescence, samples were first illuminated for 5 min with the imaging/deactivation laser at a low incidence angle to deplete fluorophores outside of the desired focal plane, and then a highly oblique illumination geometry with the incidence angle slightly smaller than the critical angle was used for activation and excitation, restricting illumination to a depth of 2–3 μm into the cell sample.

A raw data set was typically acquired in several minutes, covering an imaging volume of 81.92 μm × 81.92 μm × 750 nm without the need for sample scanning. For dual-color imaging, two channels were acquired sequentially. Alexa Fluor 647 was acquired first, since the 640 nm laser has a negligible effect on Dendra2. Afterward, Dendra2 was imaged using the excitation at 561 nm and a weak photoactivation at 405 nm, with an mCherry (excitation, 566/40; emission, 630/75) filter set. Since the absorption of Alexa Fluor 647 at 561 nm is very low (~7% of maximum), and with most of the Alexa Fluor 647 emission rejected by the mCherry filter set, the crosstalk between Alexa Fluor 647 and Dendra2 was found to be negligible. Raw data acquisition was performed with NIS-Elements AR software. Processing of single-molecule images to yield superresolution data sets were carried out by custom-developed software as described elsewhere (Shtengel et al., 2009). To extract z coordinate, a calibration curve was measured by translating the piezo z stage at 25 nm steps over 2 μm. Using gold nanoparticles as fiducials, the relationship between z and x-y ellipticity was determined as follows:

$$\varepsilon = \frac{\sigma_x - \sigma_y}{\sigma_x + \sigma_y},$$

where σ_x and σ_y are the Gaussian widths of the point-spread function. Subsequently, the ellipticity of each detected molecule was compared to the calibration curve to extract the z coordinates (Brown et al., 2011).

Superresolution images were reconstructed from the molecular coordinates by representing each molecule by a normalized 2D Gaussian whose widths correspond to σ_x and σ_ψ (Betzig et al., 2006). Single-channel 3D data are rendered with color encoding the z coordinate as described elsewhere (Kanchanawong et al., 2010).

The precision of the lateral (xy) coordinate was calculated using the following formula (Thompson et al., 2002):

$$\sigma_{x,y} = \sqrt{\frac{s^2}{N} + \frac{a^2/12}{N} + \frac{8\pi s^4 b^2}{a^2 N^2}},$$

where $\sigma_{x,y}$ is the localization uncertainty, s is the peak width, N represents photons per blinking, a is the pixel size, and b represents the background photons, and estimated from $\sim 10^6$ molecular events. The precision of the z coordinate was empirically determined from the full-width-at-half-maximum of the z position distribution histogram of isolated fluorophores observed in the samples.

Quantification of E-Cadherin Cluster Size and Density

Mean Shift Clustering

Mean shift clustering (Comaniciu and Meer, 2002) and subsequent analysis were performed in MATLAB. The algorithm is based on the multivariate kernel density function, $f(x)$, which describes the point density in certain dimensions:

$$f(\mathrm{x}) = \frac{1}{nh^d} \sum_{i=1}^{n} K\left(\frac{\mathrm{x} - \mathrm{x}_i}{h}\right),$$

where n is the number of data points; d is the dimension (in this case, $d = 2$); K is the profile of the kernel, which integrates to 1; and h defines the radius of the kernel. For each iteration, the gradient of the density estimator $f(x)$ points toward the steepest increase in density. After several iterations from randomly chosen initial points, the local maxima converged upon the cluster centers, and all accumulated points from each previous step were identified as belonging to the clusters. After all clusters were identified, the size and density of the clusters were calculated from the diameter and the number of points within each cluster, respectively.

Density Map

Square window mask of desired sizes was scanned through the data sets. The number of molecules found within each region was then used to calculate the density map. Quantification of density maps was performed by extracting the molecular densities within each 30 nm × 30 nm window from five density maps for each cell line. A Mann-Whitney nonparametric test was performed across density values from different mutants.

Identifying Adhesive and Nonadhesive Clusters

Coplating images from lateral junctions were acquired in two channels—green and red—and separately analyzed by mean shift clustering. The cluster positions from the green channel were compared with those from the red channel. If the boundary of one cluster from the green channel made contact or overlapped with any cluster from the red channel, these two clusters were considered as adhesive. Otherwise, clusters were identified as nonadhesive. A similar method was applied to the apical junctions. If the edge-to-edge distance of clusters from different channels was less than 100 nm (the length of two extended E-cadherin molecules), the two clusters were defined as adhesive. Difference in the criteria between lateral and apical junctions was due to the orientation of the junction relative to the imaging axis: apical junctions were close to perpendicular to the imaging plane, maximizing the apparent distance of the cytoplasmic tails of adjoining E-cadherins, whereas the majority of the lateral junctions were at an angle of ~15° relative to the imaging plane, resulting in an apparent overlap of the signal from E-cadherin tails in adhesive clusters.

SUPPLEMENTAL INFORMATION

Supplemental Information includes Supplemental Experimental Procedures, four figures, and one table and can be found with this article online at http://dx.doi.org/10.1016/j.devcel.2014.12.003.

ACKNOWLEDGMENTS

This work was supported by the Singapore National Research Foundation (NRF) under its NRF fellowship awarded to R.Z.-B. (NRF-RF2009-RF001-074) and P.K. (NRF-NRFF2011-04) and under its CRP grant (NRF2012NRF-CRP001-084). We thank Sergey Troyanovsky for generously sharing cell lines and Larry Shapiro and Barry Honig for helpful discussions.

Received: August 4, 2014
Revised: October 20, 2014
Accepted: December 1, 2014
Published: January 15, 2015

REFERENCES

Adams, C.L., Nelson, W.J., and Smith, S.J. (1996). Quantitative analysis of cadherin-catenin-actin reorganization during development of cell-cell adhesion. J. Cell Biol. *135*, 1899–1911.

Adams, C.L., Chen, Y.T., Smith, S.J., and Nelson, W.J. (1998). Mechanisms of epithelial cell-cell adhesion and cell compaction revealed by high-resolution tracking of E-cadherin-green fluorescent protein. J. Cell Biol. *142*, 1105–1119.

Annibale, P., Vanni, S., Scarselli, M., Rothlisberger, U., and Radenovic, A. (2011). Quantitative photo activated localization microscopy: unraveling the effects of photoblinking. PLoS ONE *6*, e22678.

Baranwal, S., and Alahari, S.K. (2009). Molecular mechanisms controlling E-cadherin expression in breast cancer. Biochem. Biophys. Res. Commun. *384*, 6–11.

Betzig, E., Patterson, G.H., Sougrat, R., Lindwasser, O.W., Olenych, S., Bonifacino, J.S., Davidson, M.W., Lippincott-Schwartz, J., and Hess, H.F. (2006). Imaging intracellular fluorescent proteins at nanometer resolution. Science *313*, 1642–1645.

Brasch, J., Harrison, O.J., Honig, B., and Shapiro, L. (2012). Thinking outside the cell: how cadherins drive adhesion. Trends Cell Biol. *22*, 299–310.

Brown, T.A., Tkachuk, A.N., Shtengel, G., Kopek, B.G., Bogenhagen, D.F., Hess, H.F., and Clayton, D.A. (2011). Superresolution fluorescence imaging of mitochondrial nucleoids reveals their spatial range, limits, and membrane interaction. Mol. Cell. Biol. *31*, 4994–5010.

Carneiro, P., Fernandes, M.S., Figueiredo, J., Caldeira, J., Carvalho, J., Pinheiro, H., Leite, M., Melo, S., Oliveira, P., Simões-Correia, J., et al. (2012).

E-cadherin dysfunction in gastric cancer—cellular consequences, clinical applications and open questions. FEBS Lett. *586*, 2981–2989.

Cavey, M., Rauzi, M., Lenne, P.F., and Lecuit, T. (2008). A two-tiered mechanism for stabilization and immobilization of E-cadherin. Nature *453*, 751–756.

Cheng, Y. (1995). Mean shift, mode seeking, and clustering. IEEE Trans. Pattern Anal. Mach. Intel. *17*, 790–799.

Chu, Y.S., Thomas, W.A., Eder, O., Pincet, F., Perez, E., Thiery, J.P., and Dufour, S. (2004). Force measurements in E-cadherin-mediated cell doublets reveal rapid adhesion strengthened by actin cytoskeleton remodeling through Rac and Cdc42. J. Cell Biol. *167*, 1183–1194.

Comaniciu, D., and Meer, P. (2002). Mean shift: A robust approach toward feature space analysis. IEEE Trans. Pattern Anal. Mach. Intel. *24*, 603–619.

Harris, T.J., and Tepass, U. (2010). Adherens junctions: from molecules to morphogenesis. Nat. Rev. Mol. Cell Biol. *11*, 502–514.

Harrison, O.J., Corps, E.M., and Kilshaw, P.J. (2005). Cadherin adhesion depends on a salt bridge at the N-terminus. J. Cell Sci. *118*, 4123–4130.

Harrison, O.J., Jin, X., Hong, S., Bahna, F., Ahlsen, G., Brasch, J., Wu, Y., Vendome, J., Felsovalyi, K., Hampton, C.M., et al. (2011). The extracellular architecture of adherens junctions revealed by crystal structures of type I cadherins. Structure *19*, 244–256.

Hess, S.T., Girirajan, T.P., and Mason, M.D. (2006). Ultra-high resolution imaging by fluorescence photoactivation localization microscopy. Biophys. J. *91*, 4258–4272.

Hirokawa, N., and Heuser, J.E. (1981). Quick-freeze, deep-etch visualization of the cytoskeleton beneath surface differentiations of intestinal epithelial cells. J. Cell Biol. *91*, 399–409.

Hong, S., Troyanovsky, R.B., and Troyanovsky, S.M. (2010). Spontaneous assembly and active disassembly balance adherens junction homeostasis. Proc. Natl. Acad. Sci. USA *107*, 3528–3533.

Hong, S., Troyanovsky, R.B., and Troyanovsky, S.M. (2013). Binding to F-actin guides cadherin cluster assembly, stability, and movement. J. Cell Biol. *201*, 131–143.

Huang, B., Wang, W., Bates, M., and Zhuang, X. (2008). Three-dimensional super-resolution imaging by stochastic optical reconstruction microscopy. Science *319*, 810–813.

Iino, R., Koyama, I., and Kusumi, A. (2001). Single molecule imaging of green fluorescent proteins in living cells: E-cadherin forms oligomers on the free cell surface. Biophys. J. *80*, 2667–2677.

Kametani, Y., and Takeichi, M. (2007). Basal-to-apical cadherin flow at cell junctions. Nat. Cell Biol. *9*, 92–98.

Kanchanawong, P., Shtengel, G., Pasapera, A.M., Ramko, E.B., Davidson, M.W., Hess, H.F., and Waterman, C.M. (2010). Nanoscale architecture of integrin-based cell adhesions. Nature *468*, 580–584.

Katz, B.Z., Levenberg, S., Yamada, K.M., and Geiger, B. (1998). Modulation of cell-cell adherens junctions by surface clustering of the N-cadherin cytoplasmic tail. Exp. Cell Res. *243*, 415–424.

Kovacs, E.M., Goodwin, M., Ali, R.G., Paterson, A.D., and Yap, A.S. (2002). Cadherin-directed actin assembly: E-cadherin physically associates with the Arp2/3 complex to direct actin assembly in nascent adhesive contacts. Curr. Biol. *12*, 379–382.

Kusumi, A., Suzuki, K., and Koyasako, K. (1999). Mobility and cytoskeletal interactions of cell adhesion receptors. Curr. Opin. Cell Biol. *11*, 582–590.

Laur, O.Y., Klingelhöfer, J., Troyanovsky, R.B., and Troyanovsky, S.M. (2002). Both the dimerization and immunochemical properties of E-cadherin EC1 domain depend on Trp(156) residue. Arch. Biochem. Biophys. *400*, 141–147.

Lee, S.H., Shin, J.Y., Lee, A., and Bustamante, C. (2012). Counting single photoactivatable fluorescent molecules by photoactivated localization microscopy (PALM). Proc. Natl. Acad. Sci. USA *109*, 17436–17441.

McEwen, A.E., Escobar, D.E., and Gottardi, C.J. (2012). Signaling from the adherens junction. Subcell. Biochem. *60*, 171–196.

McGill, M.A., McKinley, R.F., and Harris, T.J. (2009). Independent cadherin-catenin and Bazooka clusters interact to assemble adherens junctions. J. Cell Biol. *185*, 787–796.

Miyaguchi, K. (2000). Ultrastructure of the zonula adherens revealed by rapid-freeze deep-etching. J. Struct. Biol. *132*, 169–178.

Morone, N., Fujiwara, T., Murase, K., Kasai, R.S., Ike, H., Yuasa, S., Usukura, J., and Kusumi, A. (2006). Three-dimensional reconstruction of the membrane skeleton at the plasma membrane interface by electron tomography. J. Cell Biol. *174*, 851–862.

Murray, P.S., and Zaidel-Bar, R. (2014). Pre-metazoan origins and evolution of the cadherin adhesome. Biol. Open. *3*, 1183–1195.

Pertz, O., Bozic, D., Koch, A.W., Fauser, C., Brancaccio, A., and Engel, J. (1999). A new crystal structure, Ca2+ dependence and mutational analysis reveal molecular details of E-cadherin homoassociation. EMBO J. *18*, 1738–1747.

Petrova, Y.I., Spano, M.M., and Gumbiner, B.M. (2012). Conformational epitopes at cadherin calcium-binding sites and p120-catenin phosphorylation regulate cell adhesion. Mol. Biol. Cell *23*, 2092–2108.

Ratheesh, A., and Yap, A.S. (2012). A bigger picture: classical cadherins and the dynamic actin cytoskeleton. Nat. Rev. Mol. Cell Biol. *13*, 673–679.

Rust, M.J., Bates, M., and Zhuang, X. (2006). Sub-diffraction-limit imaging by stochastic optical reconstruction microscopy (STORM). Nat. Methods *3*, 793–795.

Sako, Y., Nagafuchi, A., Tsukita, S., Takeichi, M., and Kusumi, A. (1998). Cytoplasmic regulation of the movement of E-cadherin on the free cell surface as studied by optical tweezers and single particle tracking: corralling and tethering by the membrane skeleton. J. Cell Biol. *140*, 1227–1240.

Sengupta, P., Jovanovic-Talisman, T., Skoko, D., Renz, M., Veatch, S.L., and Lippincott-Schwartz, J. (2011). Probing protein heterogeneity in the plasma membrane using PALM and pair correlation analysis. Nat. Methods *8*, 969–975.

Shapiro, L., Fannon, A.M., Kwong, P.D., Thompson, A., Lehmann, M.S., Grübel, G., Legrand, J.F., Als-Nielsen, J., Colman, D.R., and Hendrickson, W.A. (1995). Structural basis of cell-cell adhesion by cadherins. Nature *374*, 327–337.

Shtengel, G., Galbraith, J.A., Galbraith, C.G., Lippincott-Schwartz, J., Gillette, J.M., Manley, S., Sougrat, R., Waterman, C.M., Kanchanawong, P., Davidson, M.W., et al. (2009). Interferometric fluorescent super-resolution microscopy resolves 3D cellular ultrastructure. Proc. Natl. Acad. Sci. USA *106*, 3125–3130.

Thompson, R.E., Larson, D.R., and Webb, W.W. (2002). Precise nanometer localization analysis for individual fluorescent probes. Biophys. J. *82*, 2775–2783.

Tokunaga, M., Imamoto, N., and Sakata-Sogawa, K. (2008). Highly inclined thin illumination enables clear single-molecule imaging in cells. Nat. Methods *5*, 159–161.

Troyanovsky, S. (2005). Cadherin dimers in cell-cell adhesion. Eur. J. Cell Biol. *84*, 225–233.

Troyanovsky, S. (2012). Adherens junction assembly. Subcell. Biochem. *60*, 89–108.

Troyanovsky, R.B., Sokolov, E., and Troyanovsky, S.M. (2003). Adhesive and lateral E-cadherin dimers are mediated by the same interface. Mol. Cell. Biol. *23*, 7965–7972.

Truong Quang, B.A., Mani, M., Markova, O., Lecuit, T., and Lenne, P.F. (2013). Principles of E-cadherin supramolecular organization in vivo. Curr. Biol. *23*, 2197–2207.

van Roy, F., and Berx, G. (2008). The cell-cell adhesion molecule E-cadherin. Cell. Mol. Life Sci. *65*, 3756–3788.

Vasioukhin, V., Bauer, C., Yin, M., and Fuchs, E. (2000). Directed actin polymerization is the driving force for epithelial cell-cell adhesion. Cell *100*, 209–219.

Wu, Y., Vendome, J., Shapiro, L., Ben-Shaul, A., and Honig, B. (2011). Transforming binding affinities from three dimensions to two with application to cadherin clustering. Nature *475*, 510–513.

Yamazaki, D., Oikawa, T., and Takenawa, T. (2007). Rac-WAVE-mediated actin reorganization is required for organization and maintenance of cell-cell adhesion. J. Cell Sci. *120*, 86–100.

Yap, A.S., Niessen, C.M., and Gumbiner, B.M. (1998). The juxtamembrane region of the cadherin cytoplasmic tail supports lateral clustering, adhesive strengthening, and interaction with p120ctn. J. Cell Biol. *141*, 779–789.

Yonemura, S., Itoh, M., Nagafuchi, A., and Tsukita, S. (1995). Cell-to-cell adherens junction formation and actin filament organization: similarities and differences between non-polarized fibroblasts and polarized epithelial cells. J. Cell Sci. *108*, 127–142.

Zaidel-Bar, R. (2013). Cadherin adhesome at a glance. J. Cell Sci. *126*, 373–378.

Zhang, Y., Sivasankar, S., Nelson, W.J., and Chu, S. (2009). Resolving cadherin interactions and binding cooperativity at the single-molecule level. Proc. Natl. Acad. Sci. USA *106*, 109–114.